


PAPER • OPEN ACCESS

Optimizing film thickness to delay strut fracture in high-entropy alloy composite microlattices

To cite this article: James Utama Surjadi *et al* 2021 *Int. J. Extrem. Manuf.* **3** 025101

View the [article online](#) for updates and enhancements.

Optimizing film thickness to delay strut fracture in high-entropy alloy composite microlattices

James Utama Surjadi^{1,3}, Xiaobin Feng^{1,3}, Wenzhao Zhou^{2,3} and Yang Lu^{1,2} 

¹ Department of Mechanical Engineering, City University of Hong Kong, Kowloon, Hong Kong Special Administrative Region of China

² Nano-Manufacturing Laboratory (NML), City University of Hong Kong Shenzhen Research Institute, Shenzhen 518057, People's Republic of China

E-mail: yanglu@cityu.edu.hk

Received 17 June 2020, revised 27 October 2020

Accepted for publication 6 January 2021

Published 25 January 2021



Abstract

Incorporating high-entropy alloys (HEAs) in composite microlattice structures yields superior mechanical performance and desirable functional properties compared to conventional metallic lattices. However, the modulus mismatch and relatively poor adhesion between the soft polymer core and stiff metallic film coating often results in film delamination and brittle strut fracture at relatively low strain levels (typically below 10%). In this work, we demonstrate that optimizing the HEA film thickness of a CoCrNiFe-coated microlattice completely suppresses delamination, significantly delays the onset of strut fracture ($\sim 100\%$ increase in compressive strain), and increases the specific strength by up to 50%. This work presents an efficient strategy to improve the properties of metal-composite mechanical metamaterials for structural applications.

Keywords: high-entropy alloy, microlattice, mechanical metamaterials, microstructure, thin film

(Some figures may appear in colour only in the online journal)

1. Introduction

Mechanical metamaterials such as metallic microlattices have attracted increasing interest in the recent years owing to its excellent mechanical properties, such as high stiffness and strength at low densities [1–7]. Among the various strategies implemented [8–17], metal/alloy composite microlattices present a straightforward and effective method to elevate the stiffness and strength at even lower weight [18–21]. Furthermore, high-entropy alloys (HEAs), consisting of four or five primary constituent metal elements, have recently

been implemented in composite micro- and nanolattices to exhibit superior specific strength and tunable properties compared to conventional metals/alloys [22–24]. Despite their high strength [22], these HEA microlattices still experience brittle strut fracture at low compressive strains ($\sim 7\%$). The majority of composite microlattices reported thus far exhibit this phenomenon, which is primarily caused by weak cores or film delamination [12, 18–20]. Hence, in this work, we employed projection micro-stereolithography (P μ SL) and magnetron sputtering to fabricate CoCrNiFe-coated composite microlattice. Due to its liquid crystal on silicon spatial light modulator and multi-projection stitching process, P μ SL offers a large, high-resolution build area, enabling the fabrication of centimeter-scale samples with micro-scale resolution [10, 25, 26]. We show that optimizing the film thickness completely suppresses delamination and drastically delays the onset of strut fracture. Ultimately, we managed to fabricate composite microlattices that exhibit higher specific strength and compressive strain compared to previous works.

³ These authors contributed equally to this work.



Original content from this work may be used under the terms of the [Creative Commons Attribution 3.0 licence](https://creativecommons.org/licenses/by/3.0/). Any further distribution of this work must maintain attribution to the author(s) and the title of the work, journal citation and DOI.

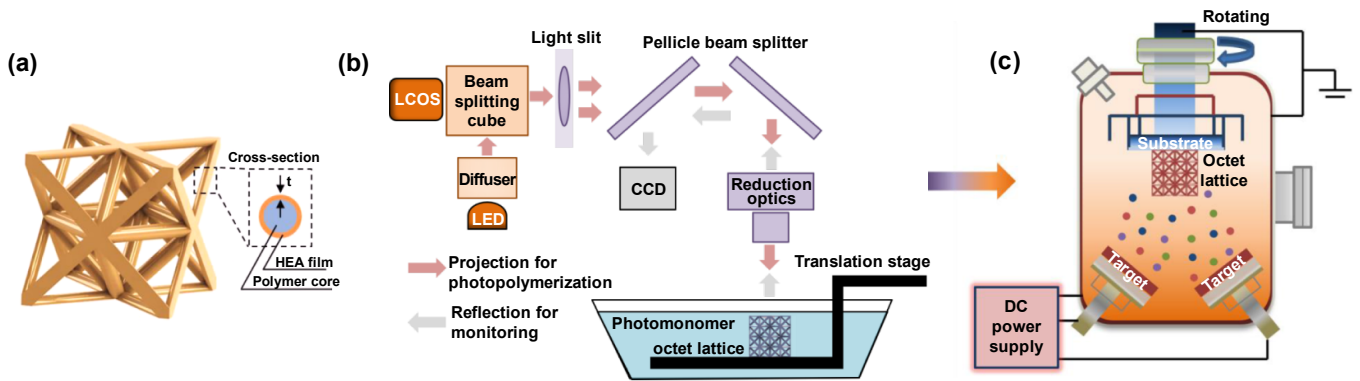


Figure 1. HEA composite lattice design and microfabrication process. (a) Representative unit cell of the HEA-coated octet lattice fabricated. (b), (c) Schematic illustration of the P μ SL printing technology (b) to fabricate the polymer lattices and DC magnetron sputtering (c) used to deposit a thin HEA coating on the polymer lattice to obtain the composite lattices.

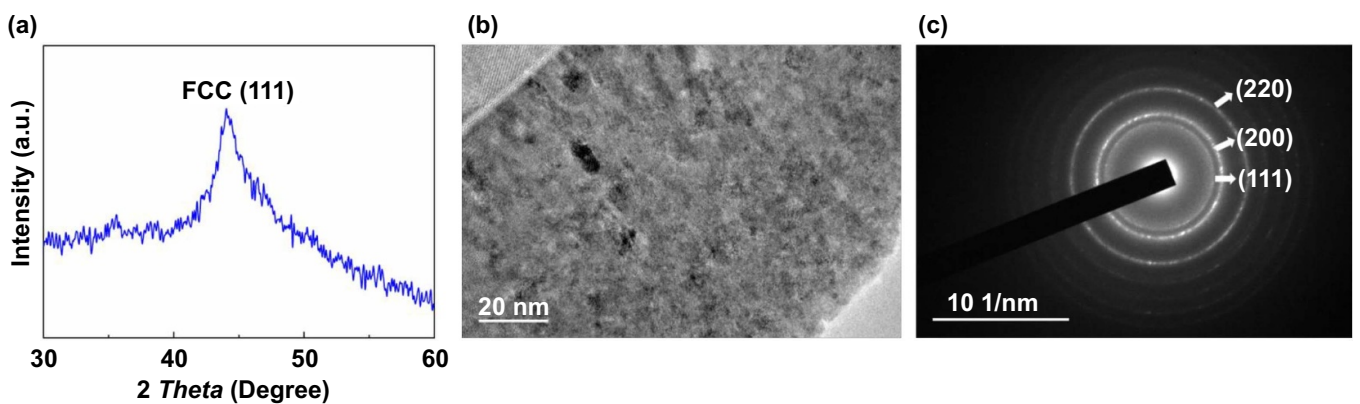


Figure 2. Microstructural analysis of CoCrNiFe HEA film. (a) XRD, (b) TEM, and corresponding (c) SADP analysis of the HEA film, confirming its FCC structure.

2. Material and methods

An octet lattice (figure 1(a)) was designed and optimized using a CAD software (SolidWorksTM). Polymer microlattices were fabricated via P μ SL (BMFTM Technologies) using 1,6-hexanediol diacrylate (HDDA) resin (figure 1(b)). The octet geometry demonstrates stretching-dominated behavior, allowing it to withstand larger loads than bending-dominated lattices at similar relative densities [27, 28]. The octet lattice had a unit cell size of 2 mm and a strut diameter of 0.2 mm. Subsequently, a thin layer of CoCrNiFe HEA film was deposited onto the polymer scaffold via magnetron sputtering at room temperature (figure 1(c)). High purity ($\geq 99.99\%$) CoCrNiFe alloy targets were used, and the chamber was evacuated below 4.0×10^{-4} Pa. The total argon flow rate was fixed at 12 sccm, and the rotation speed was 10 r min^{-1} to homogenize the alloy composition and film thickness. The sputtering power was 200 W. The substrates were neither cooled nor heated during deposition. The thickness of HEA films was adjusted by the sputtering time, while all other parameters were kept constant. GatanTM Microtest 200 was used to perform the uniaxial compression experiments at a strain rate of 10^{-3} s^{-1} .

For characterizations, FEITM Quanta 450 FEG scanning electron microscope (SEM), JEOLTM JEM-2100 F transmission electron microscope (TEM), and RigakuTM

SmartLab x-ray diffraction (XRD) with a scanning range from 30° to 60° were used to capture the post-compression microlattice morphologies and microstructures of CoCrNiFe HEA thin films, respectively. The HEA film was deposited on a Si wafer during the deposition of the microlattice [24]. The coated Si wafer was used in the characterizations described above. The TEM sample was prepared via manual milling followed by ion-milling at liquid nitrogen temperature to minimize potential ion damages. A cross-sectional view of HEA film with a single-tilt holder was observed using TEM at an acceleration voltage of 200 kV.

3. Results and discussion

Figure 2 shows the microstructural characterization of the CoCrNiFe film. The XRD results, presented in figure 2(a), show a broad diffraction peak at about $2\theta = 44.1^\circ$, indicating the (111) lattice planes of a face-centered cubic (FCC) structure. The broad peak is associated with the nano-scale grain size and distortion in the crystal lattice, caused by the random distribution of atoms of different sizes on the lattice sites. The TEM image, shown in figure 2(b), displays a nanocrystal feature. The selected area diffraction pattern (SADP) in figure 2(c), acquired from the area in figure 2(b),

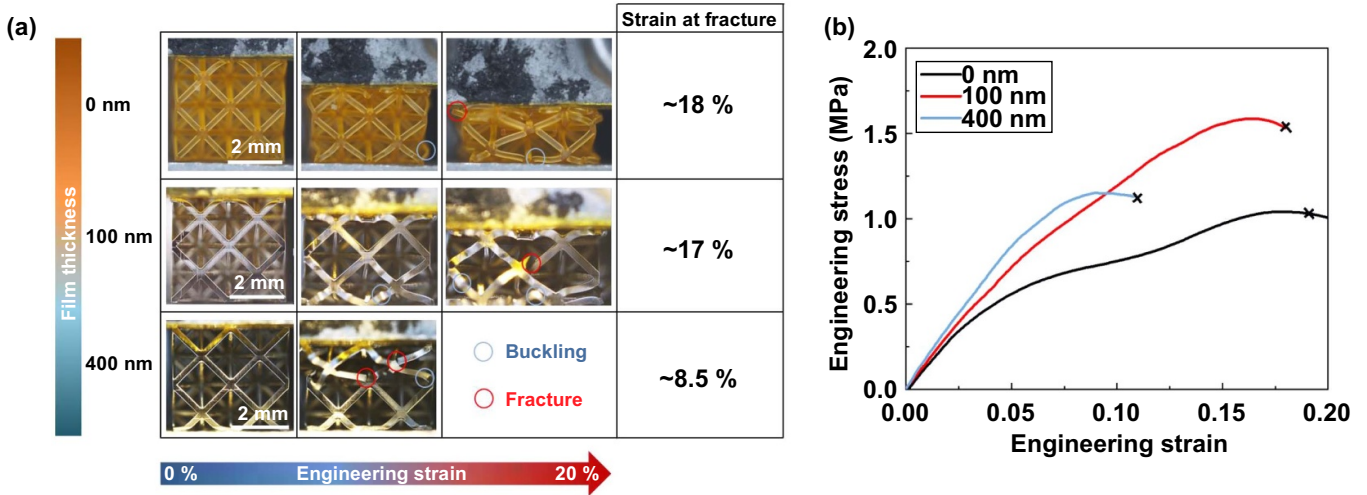


Figure 3. *In situ* uniaxial compression of polymer and composite microlattices. (a) Deformation behavior of the microlattices up to the strain at which strut fracture starts to occur. (b) Representative stress–strain curves of the polymer and composite microlattices coated with 100 nm and 400 nm of HEA film.

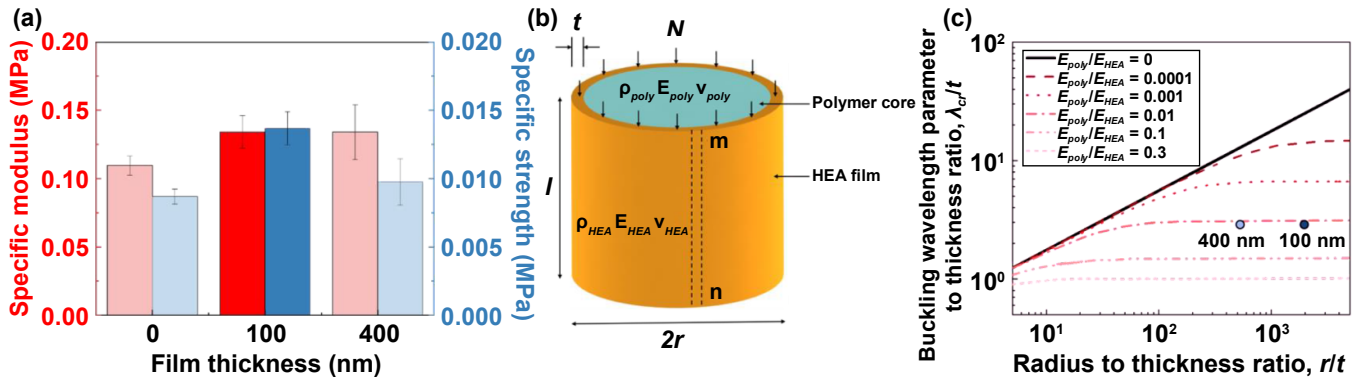


Figure 4. Mechanical analysis of the polymer and composite lattices. (a) Comparison of the specific Young's modulus and strength of the HEA-coated lattices and pure polymer. (b) Schematic illustration of the core–shell pillar under uniaxial compression used in the buckling model. (c) Plot for the buckling wavelength parameter against the radius to thickness ratio for different ratios of Young's modulus. The values for the two CoCrNiFe thicknesses used are indicated on the plot [29].

shows (111), (200) and (220) peaks, further verifying the FCC structure.

Figure 3 shows the *in situ* uniaxial compression experiments performed on the polymer and composite microlattices. Figures 3(a) and (b) show the deformation process of the microlattices during compression and the corresponding stress–strain curves, respectively. All of the microlattices in figure 3(a) show elastic strut buckling at low compressive strains. However, the microlattice with a thicker coating (i.e. 400 nm) exhibited localized strut fracture before the pristine polymer (i.e. 0 nm) and composite microlattice, which had a thinner coating (i.e. 100 nm). The thinly coated microlattice displayed strut fracture at a significantly higher compressive strain (~17%) compared to that of the composite microlattice with a thick coating (~8.5%). The thinly coated microlattice performed is similarly to the pure polymer microlattice (~18%). This observation agrees with the corresponding stress–strain curves shown in figure 3(b). Although the microlattice with a thinner coating possess a slightly lower modulus, its peak stress was about 50% higher than the

microlattice with a thick coating. The increased peak stress is due to the enhanced compressive strain at which strut fracture initiates. As shown in figure 4(a), the thinly coated microlattice possessed the highest specific modulus and strength compared to the polymer and composite microlattice with the thicker coating. The obtained values were higher than previously reported microlattices, such as NiP [3] and SiN-coated [4] microlattices. For the calculation of specific modulus and strength, the density of the composite microlattices were approximated using the following equation:

$$\rho_{\text{composite}} = \frac{\rho_{\text{HEA}} V_{\text{HEA}} + \rho_{\text{poly}} V_{\text{poly}}}{V_{\text{HEA}} + V_{\text{poly}}}$$

where ρ_{MEA} and ρ_{poly} are the estimated densities of the CoCrNiFe HEA film and HDDA photoresist, respectively. The density of the film was determined through the rule of mixtures and the respective densities of each element. V_{MEA} and V_{poly} are the volumes of the CoCrNiTi_{0.1} film and polymer core, respectively.

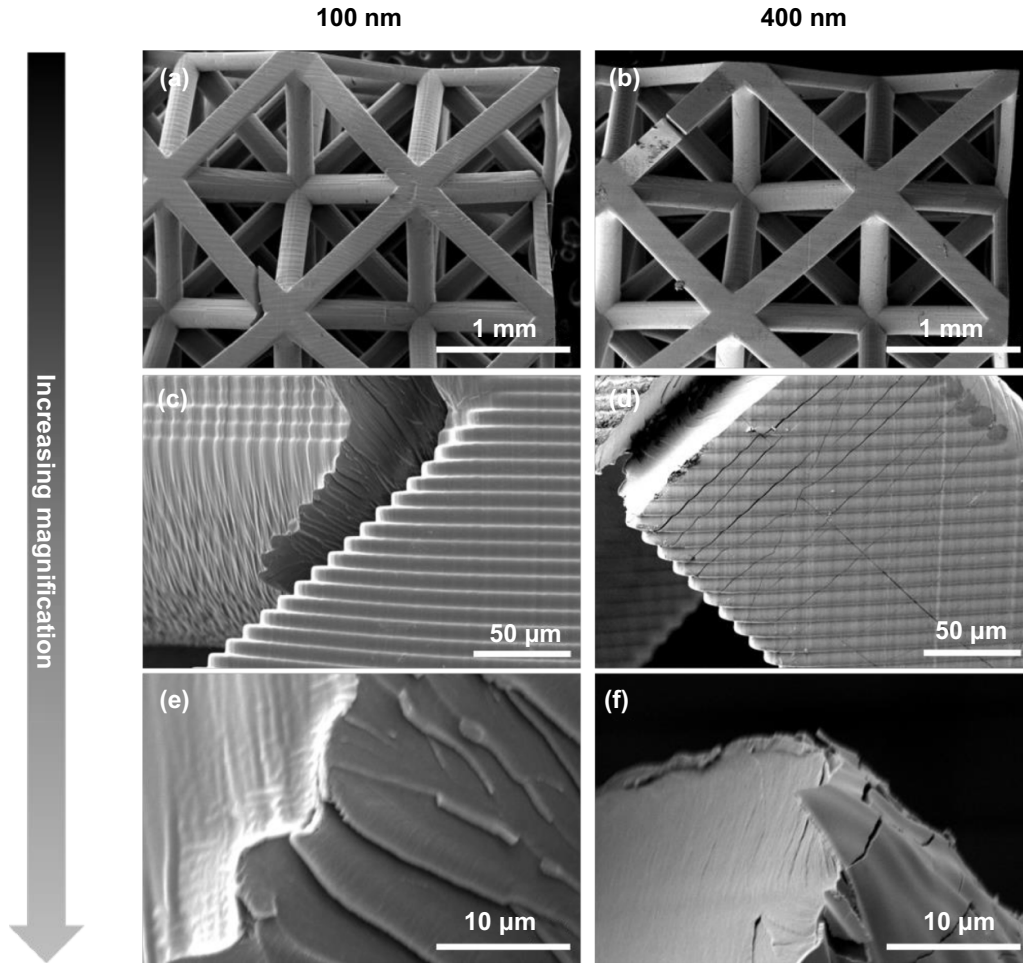


Figure 5. Post-compression SEM images of the composite microlattices with different film thicknesses (100 nm and 400 nm). (a), (b) The post-compression SEM image of an octet unit cell, (c), (d) outer fracture surface morphology, and (e), (f) cross-sectional morphology for the lattices coated with 100 nm and 400 nm of CoCrNiFe HEA, respectively.

To elucidate the delayed strut fracture in the thin-coated (i.e. 100 nm) composite microlattice, the dominant deformation behavior was determined using a simple buckling model where the composite configuration was approximated by a cylindrical shell (i.e. HEA film) with an elastic core (i.e. polymer) [29]. The loading conditions for the compression of core-shell pillars was used to mimic the stretching-dominated behavior of the octet lattice geometry [27, 30]. The critical buckling stress, σ_{cr} , for the composite pillars under uniaxial compression was calculated by modifying the results for the buckling of a hollow cylinder (equation (1)) [31] to account for an elastic, compliant core as a two-dimensional (2D) foundation supporting a longitudinal strip, mn (figure 4(b)), of the shell.

$$\sigma_o = \frac{Et}{r\sqrt{3(1-\nu^2)}}. \quad (1)$$

In equation (1), σ_o represents the critical buckling stress of a hollow cylinder with radius, r , and film or wall thickness, t . Equation (2) gives the sinusoidal radial displacement, w , during composite strip buckling:

$$w = w_m \sin\left(\frac{m\pi x}{l}\right). \quad (2)$$

In this case, l/m represents the half-buckled wavelength, l' , and w_m is the maximum radial displacement. The compliant polymer core is treated as a half elastic space with a spring constant of k_{poly} , as expressed in equation (3) [32, 33]:

$$k_{poly} = \frac{2E_{poly}}{(3-\nu_{poly})(1+\nu_{poly})} \frac{1}{\lambda} \quad (3)$$

where the buckling wavelength parameter $\lambda = l/m\pi = l'/\pi$. Consequently, the axial load (N_{axial}) in the buckled composite strip can be represented as equation (4):

$$N_{axial} = D \frac{1}{\lambda^2} + \frac{E_{HEA} t}{r^2} \lambda^2 + \frac{2E_{HEA} \alpha \lambda}{(3-\nu_{poly})(1+\nu_{poly})} \quad (4)$$

where $D = Et^3/12(1-\nu^2)$ and $\alpha = E_{poly}/E_{HEA} \cdot E_{poly}$ and E_{HEA} are the elastic modulus of the core (~ 3 GPa) and HEA film (~ 216 GPa). ν_{HEA} and ν_{poly} are the Poisson's ratio of the HEA film and core, which were taken as 0.3 and 0.4, respectively [34]. The minimum or critical buckling load can then be calculated by setting the derivative of N_{axial} with respect to λ equal to zero. In our case, $(r/t)(E_{poly}/E_{HEA}) > 10$. Thus the critical wavelength parameter, λ_{cr} , can be calculated by the

result for the wrinkling of a flat sheet (i.e. HEA film) on an elastic core (i.e. polymer), shown in the following (equation (5)) [33]:

$$\frac{\lambda_{cr}}{t} = \left[\frac{(3 - \nu_{poly})(1 + \nu_{poly})}{12(1 - \nu_{HEA}^2)} \right]^{1/3} \left[\frac{E_{HEA}}{E_{poly}} \right]^{1/3}. \quad (5)$$

For the 2D composite strip, $\sigma_{crit} = N_{axial}/t$, and as $D = Et^3/12(1 - \nu^2)$, thus, the critical buckling stress in the shell can be expressed by the following (equation (6)):

$$\sigma_{cr} = \sigma_0 f \sqrt{3(1 - \nu^2)} \quad (6)$$

where f is given by:

$$f = \frac{1}{12(1 - \nu_{HEA}^2)} \frac{(r/t)}{(\lambda_{cr}/t)^2} + \frac{(\lambda_{cr}/t)^2}{(r/t)} + \frac{3}{(3 - \nu_{poly})(1 + \nu_{poly})} \frac{E_{poly}}{E_{HEA}} \left(\frac{\lambda_{cr}}{t} \right) \left(\frac{r}{t} \right). \quad (7)$$

Alternately, by combining equations (1) and (6), the critical buckling stress, σ_{cr} , could be written as:

$$\sigma_{cr} = \frac{E_{HEA} t}{r} f. \quad (8)$$

The calculated buckling wavelength parameter to thickness ratios, λ_{cr}/t , are plotted in figure 4(c) (adapted from Karam and Gibson) [29]. Our composite microlattices lie well outside of the solid black line, indicating that the microlattices possess a core that is strong enough to support the HEA film and result in a synergistic enhancement in load bearing capability. This explains the buckling and gradual localized strut fracture observed in the deformation of our composite microlattice as opposed to the catastrophic brittle failure, represented by an extreme drop in stress levels, that results from insufficient core strength [2, 8].

The improved strength and ductility of the thin-coated composite microlattice is mainly attributed to the brittle-to-ductile transition of the HEA film caused by the size reduction. Figure 5 shows the SEM images of deformed composite microlattices after compression. The microlattice with 100 nm coating retained its smooth surface morphology without any apparent cracks even after deformation. No delamination was observed after closer inspection of a fractured strut, which indicates a good adhesion of the film to the polymer core. Furthermore, the rough and serrated cross-sectional morphology of the fractured polymer core implies that the composite microlattice has an elasto-plastic deformation behavior and experiences significant plastic deformation prior to fracture. Conversely, the microlattice with 400 nm coating had multiple cracks on its strut surfaces after compression. The cross-sectional morphology of the fractured strut indicates some delamination and brittle fracture surface, implying that it undergoes little to no plastic deformation. In a core-shell configuration, the metallic film is the dominant load-bearing component. Thus, strut fracture initiates from the film

as opposed to the polymer core (i.e. cracks start from outer surface). Once the film cracks, the polymer core cannot withstand the load by itself, causing the strut to fracture. Therefore, as the fracture expands from the HEA film to the polymer core, it travels in the direction of the slip planes of the HEA film as opposed to the build direction of the polymer. Overall, the post-mortem morphologies of the fractured lattices explain the largely delayed onset of fracture in the composite microlattices with thinner film (100 nm), which results in higher peak stress at lower densities.

4. Conclusion

In this work, we designed and fabricated CoCrNiFe HEA-composite microlattices via P μ SL 3D printing and magnetron sputtering coating. After investigating the mechanical properties of octet microlattices coated with different film thicknesses (100 nm and 400 nm) via *in situ* compression experiments, we found that reducing the HEA film coating thickness significantly delayed strut fracture onset. This increases the compressive strain at which a stress drop occurs and the strength of a microlattice despite its lower density. We attribute these results to the size-induced brittle-to-ductile transition of the HEA films, as shown by absence of cracks, delamination and obvious plastic deformation in the fractured strut of the thin-coated composite microlattices. Our strategy may apply to other advanced metallic/alloy composite microlattices designed for robust mechanical and functional applications.

Acknowledgments

The authors received funding for this work from Shenzhen Science and Technology Innovation Committee under the Grant JCYJ20170413141157573. Part of this project was supported by City University of Hong Kong (Project Nos. 9667164).

Conflict of interest

The authors declare that they have no known competing financial interests or personal relationships that influenced the work reported in this paper.

ORCID iD

Yang Lu  <https://orcid.org/0000-0002-9280-2718>

References

- [1] Fleck N A, Deshpande V S and Ashby M F 2010 Micro-architected materials: past, present and future *Proc. R. Soc. A* **466** 2495–516
- [2] Lee J H, Singer J P and Thomas E L 2012 Micro-/nanostructured mechanical metamaterials *Adv. Mater.* **24** 4782–810
- [3] Schaedler T A and Carter W B 2016 Architected cellular materials *Annu. Rev. Mater. Res.* **46** 187–210

- [4] Rashed M G, Ashraf M, Mines R A W and Hazell P J 2016 Metallic microlattice materials: a current state of the art on manufacturing, mechanical properties and applications *Mater. Des.* **95** 518–33
- [5] Yu X L, Zhou J, Liang H Y, Jiang Z Y and Wu L L 2018 Mechanical metamaterials associated with stiffness, rigidity and compressibility: a brief review *Prog. Mater. Sci.* **94** 114–73
- [6] Surjadi J U, Gao L B, Du H F, Li X, Xiong X, Fang N X and Lu Y 2019 Mechanical metamaterials and their engineering applications *Adv. Eng. Mater.* **21** 1800864
- [7] Zhang X, Wang Y J, Ding B and Li X Y 2020 Design, fabrication, and mechanics of 3D micro-/nanolattices *Small* **16** 1902842
- [8] Schaedler T A, Jacobsen A J, Torrents A, Sorensen A E, Lian J, Greer J R, Valdevit L and Carter W B 2011 Ultralight metallic microlattices *Science* **334** 962–5
- [9] Zheng X Y et al 2014 Ultralight, ultrastiff mechanical metamaterials *Science* **344** 1373–7
- [10] Zheng X Y et al 2016 Multiscale metallic metamaterials *Nat. Mater.* **15** 1100–6
- [11] Meza L R, Das S and Greer J R 2014 Strong, lightweight, and recoverable three-dimensional ceramic nanolattices *Science* **345** 1322–6
- [12] Bauer J, Hengsbach S, Tesari I, Schwaiger R and Kraft O 2014 High-strength cellular ceramic composites with 3D microarchitecture *Proc. Natl Acad. Sci. USA* **111** 2453–8
- [13] Eckel Z C, Zhou C Y, Martin J H, Jacobsen A J, Carter W B and Schaedler T A 2016 Additive manufacturing of polymer-derived ceramics *Science* **351** 58–62
- [14] Vyatskikh A, Delalande S, Kudo A, Zhang X, Portela C M and Greer J R 2018 *Nat. Commun.* **9** 593
- [15] Jackson J A et al 2018 Field responsive mechanical metamaterials *Sci. Adv.* **4** eaau6419
- [16] Bauer J, Schroer A, Schwaiger R and Kraft O 2016 Approaching theoretical strength in glassy carbon nanolattices *Nat. Mater.* **15** 438–43
- [17] Kudo A, Misseroni D, Wei Y C and Bosi F 2019 Compressive response of non-slender octet carbon microlattices *Front. Mater.* **6** 169
- [18] Zhou Y F, Yao C Z, Yang Q L, Guo L and Jiang L 2016 Mechanical properties of diamond-structured polymer microlattices coated with the silicon nitride film *Adv. Eng. Mater.* **18** 236–40
- [19] Mieszala M, Hasegawa M, Guillonneau G, Bauer J, Raghavan R, Frantz C, Kraft O, Mischler S, Michler J and Philippe L 2017 Micromechanics of amorphous metal/polymer hybrid structures with 3D cellular architectures: size effects, buckling behavior, and energy absorption capability *Small* **13** 1602514
- [20] Fan Q Q, Gao Y, Zhao Y G, Yang Q L, Guo L and Jiang L 2018 Fabrication of diamond-structured composite materials with Ni-P-diamond particles by electroless plating *Mater. Lett.* **215** 242–5
- [21] Song J, Gao L B, Cao K, Zhang H T, Xu S, Jiang C C, Surjadi J U, Xu Y M and Lu Y 2018 Metal-coated hybrid meso-lattice composites and their mechanical characterizations *Compos. Struct.* **203** 750–63
- [22] Surjadi J U, Gao L B, Cao K, Fan R and Lu Y 2018 Mechanical enhancement of core-shell microlattices through high-entropy alloy coating *Sci. Rep.* **8** 5442
- [23] Gao L B et al 2018 High-entropy alloy (HEA)-coated nanolattice structures and their mechanical properties *Adv. Eng. Mater.* **20** 1700625
- [24] Zhang X, Yao J H, Liu B, Yan J, Lu L, Li Y, Gao H J and Li X Y 2018 Three-dimensional high-entropy alloy-polymer composite nanolattices that overcome the strength-recoverability trade-off *Nano Lett.* **18** 4247–56
- [25] Zheng X Y, Deotte J, Alonso M P, Farquar G R, Weisgraber T H, Gemberling S, Lee H, Fang N and Spadaccini C M 2012 *Rev. Sci. Instrum.* **83** 125001
- [26] Ge Q, Li Z Q, Wang Z L, Kowsari K, Zhang W, He X N, Zhou J L and Fang N X 2020 Projection micro stereolithography based 3D printing and its applications *Int. J. Extreme Manuf.* **2** 022004
- [27] Deshpande V S, Fleck N A and Ashby M F 2001 Effective properties of the octet-truss lattice material *J. Mech. Phys. Solids* **49** 1747–69
- [28] O'Masta M R, Dong L, St-Pierre L, Wadley H N G and Deshpande V S 2017 The fracture toughness of octet-truss lattices *J. Mech. Phys. Solids* **98** 271–89
- [29] Karam G N and Gibson L J 1995 Elastic buckling of cylindrical shells with elastic cores—I. Analysis *Int. J. Solids Struct.* **32** 1259–83
- [30] Deshpande V S, Ashby M F and Fleck N A 2001 Foam topology: bending versus stretching dominated architectures *Acta Mater.* **49** 1035–40
- [31] Timoshenko S P and Gere J M 2009 *Theory of Elastic Stability* (North Chelmsford, MA: Courier Corporation)
- [32] Gough G S, Elam C F, Tipper G H and De Bruyne N A 1940 The stabilisation of a thin sheet by a continuous supporting medium *Aeronaut. J.* **44** 12–43
- [33] Allen H G 1969 *Analysis and Design of Structural Sandwich Panels* (Amsterdam: Elsevier)
- [34] Feng X B, Fu W, Zhang J Y, Zhao J T, Li J, Wu K, Liu G and Sun J 2017 Effects of nanotwins on the mechanical properties of Al_xCoCrFeNi high entropy alloy thin films *Scr. Mater.* **139** 71–76